Influence of Surface Roughness on Results of XPS Measurements

A. Artemenko, A. Choukourov, D. Slavinska, H. Biederman
Charles University, Faculty of Mathematics and Physics, Prague, Czech Republic.

Abstract. A concise overview of methods estimating the effect of surface roughness on results of XPS measurements is given. Tilt-angle histogram method (THM), straight-line approximation (SLA) and Monte Carlo (MC) simulations are considered. An application of such methods is described in detail in the case of flat and artificially corrugated silicon surfaces.

Introduction

The quantification of X-ray photoelectron spectroscopy (XPS) is a subject of great interest in relation to the characterization of surface properties of a wide variety of materials. The last years have seen much progress in this area of research, especially with respect to non-destructive depth-profiling, the incorporation of elastic scattering effects and the influence of instrumentation. However, quantitative XPS analyses of complex technical samples remain difficult [*Gunter et al.,* 1997].

It has been known for a long time that the effect of non-ideal surface topography strongly influences number of signal electrons in photoelectron spectroscopy and therefore distorts quantitative information. As a consequence, considerable systematic errors and possibly artifacts may be introduced when a current quantitative analysis, nondestructive concentration depth profiling or overlayer thickness is evaluated from angular-resolved spectra by models assuming an ideally flat surface [*Zemek et al.,* 2008].

The effect of roughness on the intensity of XPS signals has been studied both theoretically and by experiment by a number of authors [*Gunter et al.,* 1997]. *Fadley et al*. [1974] were the first to demonstrate that surface geometry significantly influences the spectral intensities of photoelectrons recorded at different emission angles. They showed that rough-surface intensities are equal to flat-surface intensities provided that both surfaces are clean and no X-ray shading occurs. If surface layers are present, rough-surface angular distributions deviate markedly from flat-surface distributions. Moreover, *Vutova et al.* [2001] analytically calculated the influence of surface roughness (including also the shadowing effect and the photoelectron anisotropy) for a prism-shaped corrugated surface. *Werner* [1995] studied the influence of surface roughness effects (shadowing as well as the true emission angles) on total and angle-dependent signal electron intensities. He incorporated the influence of surface roughness into an effective emission depth distribution function and found dominating influence of surface roughness over the effect of elastic scattering. The other authors analyzed rough samples by atomic force microscopy (AFM) to provide a frequency histogram of the local slopes, which is incorporated into the quantitative procedure [*Olejnik et al.,* 2005]. Several other groups investigated the influence of surface roughness on the thickness of overlayers. *Gunter et al*. [1997] expressed the uncertainty in overlayer thickness estimations by visual demonstration using error plots for fully three-dimensional model rough surface, a surface of upside-down pyramids and parts of a sphere. For both model systems they found similar error plots with valleys for emission angles of 40–45º. Applying this geometry, called the ‘‘magic angle”, the overlayer thickness on rough surfaces would be estimated with the error smaller than 10%. However, the ‘‘magic angle” has been questioned in more recent studies and requires more detail analysis.

The first part of this communication summarizes basic methods of calculations of the surface roughness effect in XPS measurements. The second part focuses on the results of investigations of random surface roughness that forms an important part of the general surface roughness on photoelectron intensity recorded from silicon samples covered by a thin silicon oxide. The Si 2p intensities measured at numerous experimental geometries were compared to the model calculations for ideally flat as well as for randomly corrugated surfaces.

Tilt-angle histogram method (THM)

The THM is based on an idea that a rough surface can be considered as consisting of small ideally flat areas [*Olejnik et al.,* 2005]. Then the total intensity $I(k)$ of photoelectrons coming from the rough

surface measured in the experimental geometry k (described below) obeys equation

$$I(k) = \int_{\alpha,\beta} T(\alpha, \beta) I(\alpha, \beta, k) \mathrm{d}\alpha \mathrm{d}\beta \quad (1)$$

where $T(\alpha, \beta)$ is the distribution function of the flat surface areas according to their normal directions determined by angles α, β, defined in Figure 1. $I(\alpha, \beta, k)$ is the intensity from an ideally flat sample of unit area with a normal direction determined by α, β

In the calculations, $T(\alpha, \beta)$ and $I(\alpha, \beta, k)$ are represented by the tilt-angle matrix, T_{ij}, and the intensity matrix, I_{ijk}. Indices i, j count angles α, β, respectively. The angular step 5º is approved in present calculations. The index k describes the position of the analyzer and the X-ray source in the angular resolved measurements.

The tilt-angle matrices T were numerically extracted from AFM height maps of the studied surfaces by a procedure described below. In Figure 2, a part of a height map of a rough surface is depicted.

The vectors $\vec{a}$ and $\vec{b}$ in the figure determine a triangular segment of the surface. The normal $\vec{n}$ of the segment can be easily calculated as vector product of $\vec{a}$ and $\vec{b}$, $\vec{n} = \vec{a} \times \vec{b}$, the area of the triangular segment is $|\vec{n}|/2$. The ij elements of the tilt-angle matrix T_{ij} are the sum of areas of segments oriented into ij direction.

The shadowing effect of signal photoelectrons by rough surface structures is accounted for by introducing the index k to the tilt-angle matrix. Then the T_{ijk} element represents an area of the sample surface that is oriented to the direction i, j and, simultaneously, it is visible from the analyzer entrance slit in the experimental geometry described by k. For the total intensity I_k in the experimental geometry k (including also the shadowing effect) holds

$$I_k = \sum_{ij} T_{ijk} I_{ijk} \quad (2)$$

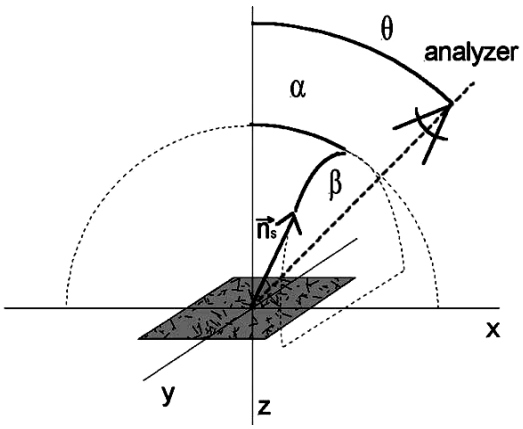

Figure 1. Experimental geometry. $\vec{n}_s$ is the local surface normal defined by angles α and β. Angle θ describes the position of the electron energy analyzer [adopted from *Olejnik et al*., 2005].

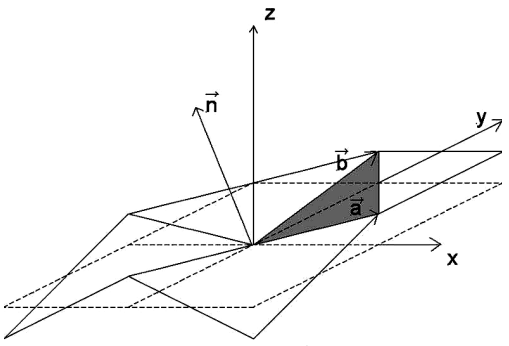

Figure 2. Sketch of a height map. Vectors $\vec{a}$ and $\vec{b}$ determine a flat triangular segment, $\vec{n}$ is the normal of the segment [adopted from *Olejnik et al*., 2005].

This equation completely separates the influence of surface roughness described by the T_{ijk} and the influence of depth distribution of elements below the surface incorporated in the intensity matrix I_{ijk}. Therefore, the I_{ijk} elements can be calculated by a common procedure valid for flat sample surfaces (analytically within Straight-line approximation (SLA), SLA corrected for elastic scattering, or by Monte Carlo (MC) calculations fully accounting electron inelastic and elastic scattering) [*Olejnik et al*., 2005].

Straight-line approximation (SLA) model for a layered sample

Let us consider two smooth thin films grown on a bulk substrate with a flat surface [*Olejnik et al*., 2005]. In particular, it is a silicon substrate, a silicon oxide film and a surface carbon contamination. Then, for the Si 2p intensity from the substrate, I_{Si}, and for the Si 2p intensity from the silicon oxide film, I_{ox}, the following equations holds

$$I_{\mathrm{Si}}(\theta) = I^{\infty}_{Si} \exp(-d_{\mathrm{ox}}/(\lambda_i^{ox} \cos\theta))\mathrm{C}(\theta) \quad (3)$$

$$I_{\mathrm{ox}}(\theta) = I^{\infty}_{ox} [1-\exp(-d_{\mathrm{ox}}/(\lambda_i^{ox} \cos\theta))]\mathrm{C}(\theta) \quad (4)$$

$$\mathrm{C}(\theta) = \exp(t/(\lambda_i^{c} \cos\theta)) \quad (5)$$

d_{ox} is the silicon oxide film thickness, t is the thickness of the surface contamination film, λ_i^{ox} and λ_i^{c} are the inelastic mean free paths of Si 2p photoelectrons in the oxide film and in the surface contamination, respectively, θ is the emission angle measured from the surface normal, I^{∞}_{f} and I^{∞}_{s} are the signal electron intensities recorded from a semi-infinite homogeneous overlayer and substrate materials, respectively. The surface contamination film brings a weakening of measured intensities by a factor given by Eq. (5). In calculations, the corresponding matrix C_{ijk} was introduced. Its elements were calculated from Eq. (5) considering again the geometry of T_{ijk}. Then, Eq. (2) for the total intensity is extended as follows:

$$I_k = \sum_{ij} T_{ijk} I_{ijk} C_{ijk} \quad (6)$$

The SLA approach can be easily (partially) corrected for electron elastic scattering effects replacing λ_i by $\lambda_{eff} = \lambda_i \lambda_{tr}/(\lambda_i + \lambda_{tr})$, where λ_{tr} is the transport mean free path [*Olejnik et al*., 2005].

Monte Carlo calculations

It is well established that elastic scattering of photoelectrons significantly affects photoelectron signal intensities and their ratios for overlayer systems. As a consequence, the substrate intensity is rather suppressed for emission angles close to the surface normal and it is reinforced at high emission angles [*Baschenko et al*., 1980]. For rough surfaces, however, both mentioned cases can influence the measured intensity in any position of the analyzer. For the above reasons, it is important to include elastic scattering phenomena into present calculations.

The calculations of intensity matrix elements I_{ijk} were carried out with the SESSA software package. The simulation is based on a partial intensity approach using the trajectory reversal algorithm. SESSA software is described by *Powell et al*. [2005]. It enables calculations of photoelectron spectral intensities for the experimental geometry used and for different predefined layered sample systems taking into account electron elastic scattering and a finite solid acceptance angle of the electron energy analyzer. The surface contamination was also introduced to the MC calculations [*Olejnik et al*., 2005].

Angular-resolved Si 2p intensities

Model calculations of Si 2p intensities for the experimental geometry used have also been described [*Olejnik et al*., 2005].

Angular dependencies of the Si 2p relative intensities, $I_{\mathrm{Si}}/I_{\mathrm{Siox}}$, measured and calculated by using Eq. (1) for flat and randomly corrugated silicon samples covered by native oxide are shown by [*Zemek et al*., 2008]. As shown in a work done by [*Olejnik et al*., 2005], experimental and calculated data for

the real corrugation are in a good agreement, while the measured data (rough-surface) and calculated (flat-surface) deviate. To describe the differences quantitatively, observed deviations are evaluated by

$$P = 100\ \frac{1}{n}\sum_{p=1}^{n}\left|\frac{I_p(\exp)-I_p(calc)}{I_p(\exp)}\right| \qquad (7)$$

I_p(exp) is the measured intensity, I_p(calc) is the calculated intensity. Summation with respect to index p is extended over all emission angles, and n is the total number of experimental intensities. Note that Eq. (7) represents an overall mean error for all angles considered.

XPS characterization of Si surfaces with different roughness

The above described semiemperical method is verified by *Zemek et al.* [2008] by the measured Si 2p angular-resolved photoelectron intensities recorded from flat and artificially corrugated silicon surfaces covered by a native silicon oxide film and a carbon contamination on the top surface.

Two silicon surfaces with *rms* (root mean square) values of 4.9 nm (sample labeled D1) and 6.3 nm (sample labeled A4) were prepared by an anodic oxidation of smooth Si(100) substrates in a mixture of ethyleneglycol (89.6%), potassium nitrate (0.4%) and water (10%). Oxidation at voltages of 100–220 V produced different values of roughness at the Si/SiO_2 interface. After oxidation, the oxide layer was dissolved by hydrofluoric acid leaving a silicon surface corrugated. Due to an air-exposure, a native silicon oxide of 1.5 nm was grown on both sample surfaces. The surface topography was investigated by using AFM Explorer (Veeco) in a non-contact mode with a sharpened tip (tip radius < 10 nm, apex ratio 1:10). The samples undergoing no further treatment were then transferred into ADES 400 angle-resolved photoelectron spectrometer (V.G. Scientific UK).

Photoelectrons were collected by a hemispherical analyzer with a small conical acceptance angle. The half-cone angle of the analyzer was 4.1º. The Si 2p photoelectron spectra were recorded at pass energy of 100 eV. Oxide and substrate spectral contributions were separated by fitting two Gaussian functions and Shirley inelastic background. The oxide thickness was estimated from a fit of the calculated angular dependencies to those measured.

Typical AFM height maps taken from surface areas of $5\times5\ \mu m^2$ of the samples A4 and D1 are shown in Figure 3.

The I_{ijk} matrix elements of photocurrent were calculated by a common procedure valid for a flat surface by MC calculations fully accounting electron inelastic and elastic scattering using SESSA software package. The matrices *T* were numerically extracted from the AFM height maps of the studied surfaces by means of histograms of the local area distribution of slopes.

Angular dependencies of the Si 2p relative intensities, I_{Si}/I_{Siox}, measured and calculated by using Eq. (2) for the flat and randomly corrugated silicon samples covered with a 1.5 nm native oxide, are shown in Figure 4.

The measured dependence has agreed well with the calculated data. Deviations between the experimental and calculated data were evaluated by Eq. (7). The results are summarized in Table 1.

The differences between the measured (rough-surface) and the calculated (flat-surface) dependencies reached about 17% for both samples in the angular interval of 0º–80º. In a more common angular range in practice, 0º–60º, the difference decreased to 4% and 6%. As expected, the differences between the measured (rough-surface) and the calculated (rough-surface) dependencies reached lower values in the angular interval of 0º–80º, about 7 % (D1) and 11% (A4). The difference reached approximately the same value for D1 and slightly lower value 9% (A4) in the narrower angular interval.

There have been several attempts to approximate the distribution of slopes by a single correcting parameter, by a mean steepness or an actual surface area. The nature of the differences in the angular dependencies in Figure 4 can be followed in Figure 5 where an error map is exemplified. It is calculated for many strictly randomly corrugated silicon surfaces (using exactly Gaussian distribution of local area slopes of different FWHM values).

For the narrow spread, below 35º, the error due to the surface topography is less than 10%. The higher error values found also for oblique emission angles are in agreement with results of simultions (Figure 4, Table 1). The vertical line indicates the position of the predicted ‘‘magic angle”. Obviously, the zero-error-line is shifted towards higher emission angles, 55º–70º, and depends on the spread of

the distribution. Values of the ‘‘magic angle” derived from the Si 2p angular dependencies, 48º and 58º for samples D1 and A4, respectively, slightly differ from those derived from Figure 5. The difference confirms the dependence of the ‘‘magic angle” values on the surface topology, as also pointed out by *Gunter et al.* [1997] and *Kappen et al.* [2000].

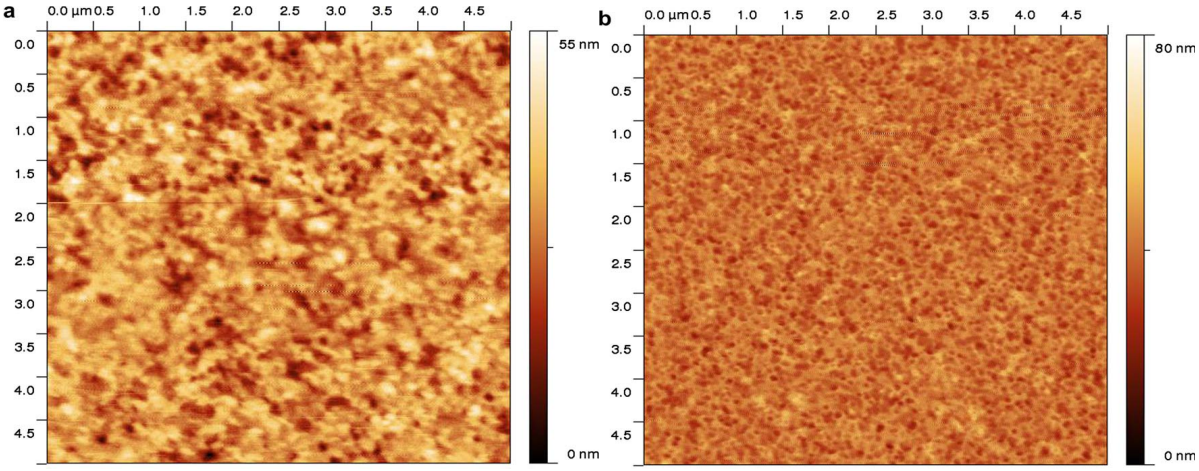

Figure 3. AFM maps typical for the sample surface A4(a) and D1(b) [adopted from *Zemek et al*., 2008].

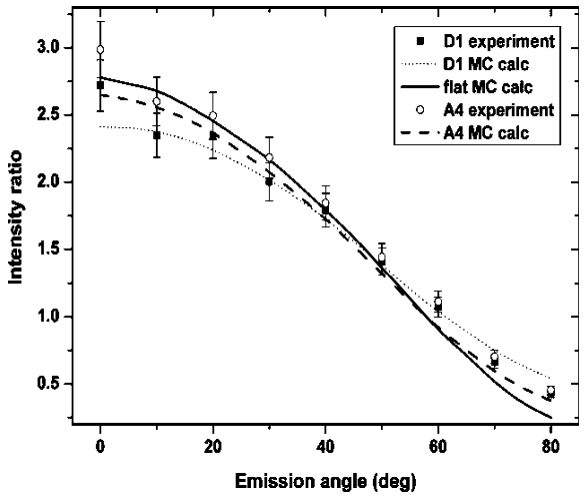

Figure 4. Measured (symbols) and calculated (lines) Si 2p angular dependencies of relative photoelectron intensity, I_{Si}/I_{Siox}, recorded on samples A4 and D1. Full line – MC calculations for ideally flat surface, dashed line – MC calculations for the randomly corrugated sample A4, and dotted line – MC calculations for the randomly corrugated sample D1 [adopted from *Zemek et al*., 2008].

Table 1. Parameters characterizing the surface topography of the samples under analysis and the angular dependencies of the normalized Si 2p intensities

Sample	Roughness, *rms* (nm)	Angular range (º)	*P** (%)	*P*** (%)	FWHM (º)	Magic angle (º)
D1	4.9	0–80 0–60	16.4 4.0	6.7 6.9	40	48
A4	6.3	0–80 0–60	17.8 6.3	11.1 8.8	26	58

*P** is the difference between the measured (rough-surface) and the calculated (flat-surface) angular dependence, *P*** is the difference between the measured (rough-surface) and the calculated (the same rough-surface) angular dependence. FWHM is the angular spread of the strictly Gaussian histogram of local area distributions of slopes. Values of the ‘‘magic angle” are extracted from the Si 2p angular dependencies as an intercept point of the flat-surface and the rough-surface dependencies displayed in Figure 4 [adopted from *Zemek et al*., 2008].

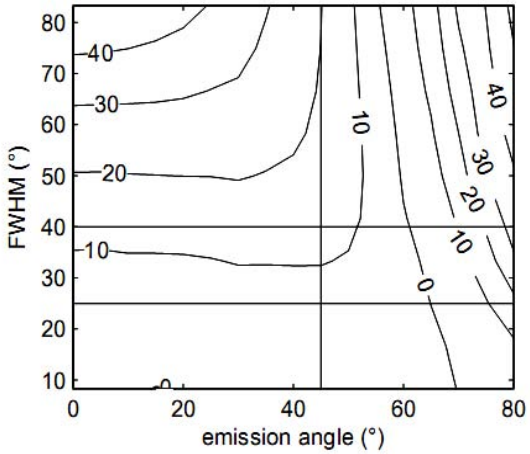

Figure 5. Error map illustrating the influence of random surface roughness on the resulted deviation calculated for silicon surface covered by a 1.5 nm native oxide. The *y*-axis expresses the angular spread (FWHM) of the histogram of the local area distribution of slopes. Two horizontal lines enclose the roughness of samples A4 (bottom line) and D1 (top line), the vertical line indicates the position of the predicted ‘‘magic angle.” Error values are in percent of the oxide thickness [adopted from *Zemek et al*., 2008].

Merzlikin et al. [2008] compared two methods, angular-resolved X-ray induced photoelectron spectroscopy (ARXPS) and excitation energy variation in photoelectron spectroscopy (ERXPS), to obtain concentration depth-profiles of elements in the near-surface region of model samples – self-assembled monolayers of n-octadecanethiol (‘‘C18- SAM”) adsorbed on gold substrates of different surface roughness. With ARXPS, roughness smoothes out the angular dependence of the intensities, which results in underestimation of the layer thickness. ERXPS offers the advantage to be performed at normal emission where deviations of the photoemission angle (by sample misalignment or surface roughness) have only minor influence on the depth coordinate. Compared with single experiments at low excitation energies, ERXPS has the advantage of utilizing a larger set of experimental information for the description of the properties at the external surface. While validated here with an idealized overlayer–substrate system, ERXPS offers an attractive potential also for the analysis of the outmost surface layers of real materials (alloys, mixed oxides, supported catalysts) irrespective of the surface roughness [*Merzlikin et al*., 2008].

Conclusions

In this work, a review of semi-empirical methods that estimate the influence of surface roughness on results of XPS measurements was done. On the example of influence of the random surface roughness on the Si 2p photoelectron intensities, it was reviewed that the measured value of roughness strongly depends on the angular spread of the local area distribution of slopes and is moderately dependent on the experimental geometry, namely for emission angles from 0º to 60º with respect to the surface normal. The error induced by the random surface corrugation can be acceptably low for a narrow spread of the local area distribution of slopes. It is further discussed that the ‘‘magic” angle, the off-normal emission angle at which the error of an overlayer thickness estimation caused by the surface roughness reached a minimum, depends on the angular spread of the local area distribution of slopes.

References

Baschenko O.A., Nefedov V.I. Relative intensities in X-ray photoelectron spectra: Part VII. The effect of elastic scattering in a solid on the angular distribution of photoelectrons escaping from samples covered with thin films of various thicknesses, *J. Electron Spectrosc. Relat. Phenom*., 21, 153-169, 1980.

Fadley C.S., Baird R.J., Novakov T., Bergstrom S.A.L. Surface analysis and angular distributions in x-ray photoelectron spectroscopy, *J. Electron Spectrosc. Relat. Phenom*., 4, 93-137, 1974.

Gunter P.L.J., Gijzeman O.L.J., Niemantsverdriet J.W. Surface roughness effects in quantitative XPS: magic angle for determining overlayer thickness, *Applied Surface Science*, 115, 342-346, 1997.

Kappen P., Reihs K., Seidel C., Voetz M., Fuchs H. Overlayer thickness determination by angular dependent X-ray photoelectron spectroscopy (ADXPS) of rough surfaces with a spherical topography, *Surface Science*, 465, 40-50, 2000.

Merzlikin S., Tolkachev N., Strunskus T., Witte G., Glogowski T., Woll C., Grunert W. Resolving the depth coordinate in photoelectron spectroscopy – Comparison of excitation energy variation vs. angular-resolved XPS for the analysis of a self-assembled monolayer model system, *Surface Science*, 602, 755-767, 2008.

Olejnik K., Zemek J., Werner W.S.M. Angular-resolved photoelectron spectroscopy of corrugated surfaces, *Surface Science*, 595, 212-222, 2005.

Powell C.J., Jablonski, A., Werner W.S.M., Smekal W. Characterization of thin films on the nanometer scale by Auger electron spectroscopy and X-ray photoelectron spectroscopy, *Appl. Surf. Sci*., 239, 470-480, 2005.

Vutova K., Mladenov G., Tanaka T., Kawabata K. Photoelectron signal simulation from textured samples covered by thin film, *Vacuum*, 62, 297-302, 2001.

Werner W.S.M. Magic Angle for Surface Roughness in XPS/AES Intensitity Ratios, *Surf. Interf. Anal*., 23, 696, 1995.

Zemek J., Olejnik K., Klapetek P. Photoelectron spectroscopy from randomly corrugated surfaces, *Surface Science*, 602, 1440-1446, 2008.

Zemek J. Comment on ‘‘Resolving the depth coordinate in photoelectron spectroscopy – Comparison of excitation energy variation vs. angular-resolved XPS for the analysis of a self-assembled monolayer model system” by S.V. Merzlikin et al. [Surf. Sci. 602 (2008) 755], *Surface Science*, 602, 3632-3633, 2008.